A Sustainable Paradigm of RIS-Aided Cell-Free MIMO for IoT Networks

Original Scientific Paper

Ismail Sharhan Baqer*
Dept. Electrical Engineering, University of Wasit, Iraq
isharhan@uowasit.edu.iq

Hasan Fahad
Dept. Electrical Engineering, University of Wasit, Iraq
hfahad@uowasit.edu.iq

Nibras Hazim Abbas
Dept. Electrical Engineering, University of Wasit, Iraq
niabbas@uowasit.edu.iq

Basim Khalaf
Dept. Electrical Engineering, University of Wasit, Iraq
bkhalaf@uowasit.edu.iq

Ahmed Abdulameer Naser
Dept. Electrical Engineering, University of Wasit, Iraq
Ahmed.Abdulameer@uowasit.edu.iq

*Corresponding author

Abstract *– Cell-free (CF) large multiple-input multiple-output (MIMO) with reconfigurable intelligent surfaces (RIS) systems and energy harvesting (EH) have garnered considerable attention in the development of 6G Internet of Things (IoT) networks. To tackle the joint optimization difficult problems, the study first develops a block coordinate alternating optimization to decompose the problem into multiple smaller sub-problems. The proposed alternating optimization algorithm with the Intermediate Value Theorem (IVT), namely AO-IVT, efficiently solves the non-convex task. Simulations verify that the deployment of RISs in CF-IoT scenarios improves the IoT connectivity, and the proposed joint design can further improve this connectivity. For instance, compared to a conventional situation (equal power and random phase shift) for a 5% anticipated rate outage, the suggested method shows a notable improvement of over 83% in terms of minimum target rate (increase from 0.24 to 1.5 nat/s/Hz) in a particular condition.*

Keywords: *wireless transfer of information and energy, Riemannian manifold, cell-free network, max-min fairness, reconfigurable intelligent surface*

Received: March 4, 2026; Accepted: April 20, 2026

1. INTRODUCTION

Conventional cellular systems have intrinsic drawbacks such as high infrastructure costs, cell-edge effects, inter-cell interference, and substantial cell-free multiple-input multiple-output (CF-MIMO) appears as a potential technique to address these issues. Several base stations (BS) are dispersed throughout the coverage region under this paradigm, efficiently serving a number of consumers [1,2]. By lowering the distance separating devices and the BSs in their immediate vicinity, this strategy promotes macro-diversity and lessens route loss [3,4]. Recent developments have improved system performance by smoothly integrating reflecting surfaces or Reconfigurable intelligent surfaces (RIS) into wireless networks. Significantly, a reflecting surface can alter radio signals at the electromagnetic scale, eliminating the need for digital signal processing methods and power amplifiers [5,6]. The potential of reflecting surfaces in the environment of CF-MIMO WTIE networks has been largely untapped, despite the fact that their implementation has unquestionably improved the energy harvesting (EH) performance in a variety of settings. Furthermore, the core technologies supporting RIS and their various uses in the Internet of Things (IoT), automotive, drone, and marine communication sectors were examined by S. Han *et al*. [7].

2. RELATED WORK

Studies in CF-MIMO systems, energy harvesting techniques, and communications using RIS have received considerable attention from researchers. However, much remains to be explored regarding the relationship between these three areas: the combined optimization of phase values in RIS systems, LSFD parameters, uplink power control, and downlink power aggregation for maximal and minimum fairness. This subsection provides a critical analysis of some key studies conducted in these areas.

Peng *et al*. suggested a cell-free radio network in [8] that uses an IRS as a secondary transmitter. The main

transmission from CF-MIMO and the secondary backscatter from IRS work at the same time in the same time-frequency bands. The authors devised a combined optimization of active beamforming in the base stations and passive beamforming in the IRS to reduce the bit error rate while maintaining low power levels. It was solved by alternating optimization, and the results of the simulation were shown for 4 BSs, 4 users, and 32 RIS elements. At 15 dB SNR, the proposed method had a BER of about 10^{-4}, which was two orders of magnitude better than the standard no-RIS baseline. On the other hand, there were no limits to energy harvesting, phase transitions in RIS were treated as continuous variables, equity between the maximum and minimum of IoT devices was not taken into account, and LSFD processing was not used.

Zeping *et al*. [9] investigated RIS-enabled CF-MIMO utilizing reflection pattern modulation. In this type of scheme, the RIS reflection patterns directly modulate the information, which lets you send more data without needing more RF chains. The authors found closed-form solutions for outage probability and ergodic rate with Rician fading, regardless of whether the channel state information (CSI) was optimal or not. Monte Carlo simulations with 10 APs, 5 users, and 50 RIS elements confirmed the formulas that were found. Compared to regular RISs with a 10 dB SNR, the algorithm increases the sum rate by 40% when there are outages. The study primarily concentrated on outage probability and ergodic rate analysis, neglecting optimization, power control, and LSFD optimization; energy harvesting was also not addressed; max-min fairness was overlooked; and phase constraints on the RIS were disregarded.

Han *et al*. [7] did a complete study on the uses of RIS in mobile communications, focusing on things like vehicle-to-everything, and the Internet of Things. The researchers in the survey have divided the literature on RIS into groups based on the application area, channel modeling, and optimization method used. They emphasized that while robust designs and the segmentation of phase shift control are essential features of practical systems, most current research on RIS optimization relies on the assumption of continuous phase shifts and accurate channel state information (CSI). Therefore, this study serves as a valuable guide for future RIS research. However, as it is merely a review paper, it does not introduce any new methods or numerical results.

Aine *et al*. [10] used tools from random array theory to study the performance of the asymptotic signal-to-noise ratio. They validated their theoretical results by conducting a simulation using 50 access points, 10 users, and 4 antennas per access point. They found that the LSFD is very close to the SINR performance achievable with a centralized MMSE scheme in a line-of-sight environment, with a difference of only 0.5 dB. Thus, this work demonstrates that the LSFD is superior in this respect. However, this evidence does not address the issue of power pooling, nor does it focus on maximal-minimum fairness optimization.

Khalil *et al*. [11] proposed an architecture for energy harvesting by CF-MIMO UAVs, aided by RIS. In the proposed system, a twofold optimization approach is presented, wherein RIS phases are controlled to optimize the minimum energy collection, and the trajectory of UAVs is optimized to minimize energy expenditure. In simulations conducted with 4 APs, 8 IoT devices, and 64 RIS elements, the suggested approach boosts the minimum energy collection by 45% and prolongs the lifetime of IoT devices by 3.2 times. Nevertheless, in the above system, no LSFD approach is applied, the energy-harvesting mechanism is linear, no saturation effect is taken into account, no max-min rate fairness is assumed, and the objective is energy-harvesting only.

Mohammed *et al*. [12] proposed a hybrid beamforming scheme for mmWave networks using Riemannian geometry. In this study, a framework and application of Riemannian manifold optimization approach under the constraint of unit modulus for hybrid analog/digital beamforming are proposed. Retraction is performed after projecting the Euclidean gradient onto the tangent space of the complex circle manifold. For simulation with 64 BS antennas, 4 RF chains, and 8 users, the Riemannian optimization approach provides up to 95% of the fully digital solution with only 8 times the computational cost of the SDR approaches. However, the approach is restricted to the downlink, targets mmWave hybrid beamforming only, and does not include energy harvesting or LSFD.

The above-mentioned analysis and literature review highlight the necessity of studying the CF-MIMO WTIE method's efficiency in self-powered IoT networks. In the present paper, the AO-IVT scheme optimizes all four components together for the min-max rate problem: uplink powers, LSFD coefficients, downlink energy harvesting beamforming, and phase shifts of discontinuous RIS elements. In particular, it employs a nonlinear sigmoidal EH function, imposes the discrete nature of phase shifts using the Riemannian manifold approach, incorporates LSFD into RIS optimization, and presents a complete ablation study that analyzes the contribution of each feature. In contrast to the approach in [8], where the bit error rate of the communication system is optimized, this paper explores an RIS-assisted CF-MIMO system to maximize the minimum rate of IoT devices, or, alternatively, the minimum SINR under device-specific and aggregate transmit power constraints. As all the uplink power allocation, receive combining vectors, and RIS phase shifts are coupled in the min-max rate problem, its solution becomes highly non-convex and hard to solve. To attain a scalable solution, the task is reformulated by introducing a slack variable (SINR threshold) and solving it via an alternating optimization framework combined with bisection search, where each iteration consists of convex second-order cone programming (SOCP) subproblems with respect to one variable block while fixing the others. The main contributions of the research are as follows:

- Provides a unified alternating optimization framework that addresses the aforementioned challeng-

es, where the suggested LSFD-based algorithm exploits second-order cone programming (SOCP) for efficient uplink power control and downlink EH feasibility checks. The algorithm leverages the Intermediate Value Theorem (bisection search over the min. SINR target) with certified convergence via monotonic feasibility properties.

- Introduces the complexity analysis and demonstrates the performance gains over benchmarks' schemes, where the algorithm's efficiency is validated for different system parameter settings by numerical simulation results.

3. SYSTEM MODEL

Network Architecture: The considered model consists of a cell-free massive MIMO network with B base stations (BS), each provided with M antennas, serving K IoT- single-antenna devices. An RIS with N passive intelligent elements is deployed to enhance both uplink communication and downlink wireless power transfer. As seen in Fig. 1, each BS is supported by R numbers of RISs, each surface is made up of N passive reflective segments, and the Central Processing Unit (CPU) controls these RIS units via wired or wireless back-haul. The transmission from BSs to devices is managed by the TDD technique, which includes two steps for each coherence period: the uplink training phase (UL) and the downlink information dispatch (DL). A complex matrix of $F \in C^{M\times K}$ represents the direct route to the k^{th} IoT-device, $h \in C^{N\times 1}$ represents the RIS-IoT-device route, and a channel complex matrix H of dimension $C^{M\times N}$ represents the pathways between the BSs and the intelligent reflecting surfaces. The diagonal matrix represents the phase-shifting matrix of the gathered signal at the intelligent reflecting surface $\phi_r \in C^{N\times N}\ \forall\ r \in R$ [12]:

$$\phi r = diag(e^{j\theta r1},\ldots,e^{j\theta rN}), \tag{1}$$

Hence, the expression for each part of the analog-phase shifter is $\theta_{rn} \in [0, 2\pi)$ represents the discrete phase-shift levels. This study considered a discrete value (a finite number) for the phase shift angles of intelligent surface segments in order to simplify the practical implementation. If the level numbers or phase-shifting precision are represented by b-bits, the number of these levels will be 2^b.

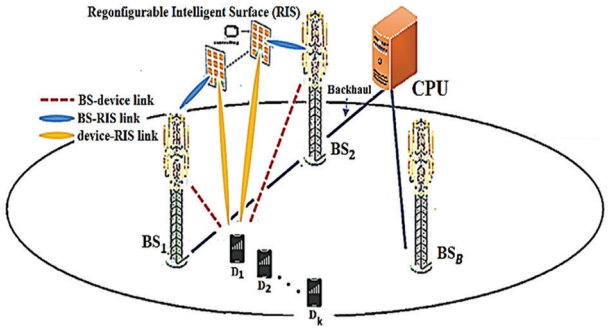


Fig. 1. A schematic of a multi-RIS-assisted CF-MIMO self-powered IoT network

To keep things simple, the current study additionally assumed that the phase shifter levels were uniformly quantized in the range of $[0;2\pi]$. Finally, the discrete phase shift values set for a single RIS element can be written as follows [12]:

$$\theta_{rn} \in \left\{0,\ \frac{\pi}{2^{b-1}},\ \ldots,\ (2^b-1)\frac{\pi}{2^{b-1}}\right\}, \forall\ r \in R\ \&\ n \in N \tag{2}$$

Theoretically, the elements' amplitude of reflection C_{rn} can be changed for some reasons, including system efficiency optimization and CSI measurement. Nevertheless, it is fundamentally costly to consider an independent control strategy for both the phase shifter and the reflection amplitude simultaneously. Therefore, an individual reflecting segment is typically considered to enhance the signal's phase shift for the sake of a simple implementation. For every K IoT-devices at the b^{th} BS, the transmitted baseband unit variance signal vector x_r, can be stated as follows, $x_r = \sum_{k\in|K|} v_{rk}\ S_k$, where, the vector $V_{bk} \in C^{B\times K}\ \forall\ b \in B$, is the BS active beamformer for the k^{th} IoT device, and S^k is the data to be delivered to the k^{th} device. The channel between BS b and IoT-device k is modeled as, $F_{bk} = \sqrt{\beta_{bk}}\, g_{bk}$, where β_{bk} is the large-scale fading coefficient and $g_{bk} \sim CN(0, I_M)$ is the small-scale fading component. Additionally, for the two components RIS-assisted channel, let's use the symbol Q_{bk} to represent the total effective or aggregate cascading channel from device k to BS b through RISs belonging to BS b as follows [12]:

$$Q_{bk} = F_{bk} + G_k\, \phi_r \tag{3}$$

Here, $F_{bk} \in C^M$ is the direct channel component from BS b to the IoT-device, $G_k = H_r diag(h_{r,k}) \in C^{M\times N}$ models the cascaded IoT-device-RIS-base station channel, with H_r being the RIS-to-base station channel and $h_{r,k} \in C^{N\times 1}$ is the channel from reflecting surface to IoT-device k. In addition, to simplify the notation and mathematical expression, stack across BSs to describe the overall effective channel to all BS's antennas as $Q_k \in C^{BM\times 1}$ formed by stacking the channels, Q_{1k}, Q_{2k},..., Q_{Bk}. All the IoT devices transmit a unity variance symbol s_k, each with transmit powers p_k, consequently, the received signal across all BSs can be given as follows, $y = \sum_{k\in|K|} Q_k \sqrt{p_k}\ s_k + n$, where, p_k is the transmit power of device k, $s_k \sim CN(0,1)$ is the transmitted symbol, and $n \sim CN(0, \sigma^2 I_{BM})$ represents the additive noise. It's crucial to keep in mind that the time-division duplex protocol-based uplink-pilot sequences from IoT devices can be utilized to evaluate the downlink (DL) channel utilizing the channel's reciprocity technique. Compressive sensing (CS) based on the sparse features of the cascaded channel or the linear minimum mean square error technique can be used to obtain the channel state information (CSI) by establishing the RIS-assisted linkage through the cascaded channel.

3.1. UPLINK SIGNAL MODEL AND LSFD

For the uplink signal decoding, a two-stage processing is employed, the first is the BS local MMSE combining and the second is the CPU distributed LSFD decoding [9].

Optimizing local combiners v_{bk} (MMSE): Based on pilot estimates for the IoT-device k, BS b forms the Local MMSE combiner via maximizing the instantaneous uplink SINR at this BS independent of the other BSs as follows:

$$\begin{aligned}\mathbf{v}_{bk}^{\star} &= \underset{\mathbf{v}_{bk}}{\operatorname{argmin}}\mathbb{E}\left[\|s_k - \mathbf{v}_{bk}^H\mathbf{y}_b\|_F^2\right] \\ &= \underset{\mathbf{v}_{bk}}{\operatorname{argmin}}\{p_k - p_k\mathbf{v}_{bk}^H\mathbf{Q}_{bk} - p_k\mathbf{Q}_{bk}^H\mathbf{v}_{bk}\end{aligned} \tag{4}$$

$$+\mathbf{v}_{bk}^H\left(\sum_{i\in|K|,i\neq k} p_i\,\mathbb{E}\{\mathbf{Q}_{bk}\mathbf{Q}_{bi}^H\} + \sigma_k^2\mathbf{I}_M\right)\mathbf{v}_{bk}\} \tag{5}$$

Setting gradient w.r.t v_{bk} to zero, $(\partial(.))/(\partial_{v_{bk}})=0$, yields:

$$-p_k\mathbf{Q}_{bk} + \left(\sum_{i\in|K|,i\neq k} p_i\,\mathbb{E}\{\mathbf{Q}_{bk}\mathbf{Q}_{bi}^H\} + \sigma_k^2\mathbf{I}_M\right)\mathbf{v}_{bk} = 0 \tag{6}$$

$$\mathbf{v}_{bk}^{mmse} = p_k\Big(\sum_{i\in|K|,\,i\neq k} p_i\,\mathbb{E}\{\mathbf{Q}_{bk}\mathbf{Q}_{bi}^H\} + \sigma_k^2\mathbf{I}_M\Big)^{-1}\,\mathbf{Q}_{bk} \tag{7}$$

Then, each BS computes the vector of locally combined uplink signals for IoT-device k: $\hat{s}_{b,k}=v_{bk}^{mmse}\,y_b$. For the second stage, each BS sends the vectors $v_{bk}^{H}\,Q_{bi}$ to CPU for LSFD process. With linear MMSE combining, most interference is suppressed locally, while LSFD mainly exploits macro-diversity across BSs.

Distributed LSFD process at the CPU: Each BS applies a local linear combiner $v_{bk}\in C^M$ to its local received vector to produce a scalar local estimate for IoT-device k, then the CPU performs the weighted combining through collecting of the vectors $\hat{s}_{b,k}$ from all BSs: $\hat{s}_k=\sum(b\in|B|)\,a_{bk}\,\hat{s}_{b,k}=a_k^{H}\,s_k$, where $a_{bk}\in C$ are LSFD coefficients collected in $a_k\in C^B$. Next, after applying LSFD vector a^k, the estimated signal is:

$$\hat{s}_k = \mathbf{a}_k^H\hat{\mathbf{s}}_k = \sqrt{p_k}\mathbf{a}_k^H\mathbf{Q}_k s_k + \sum_{i\neq k}\sqrt{p_i}\,\mathbf{a}_k^H\mathbf{Q}_i s_i + \mathbf{a}_k^H\mathbf{n} \tag{8}$$

given that, $a_k=[a_{1k},\ldots,a_{Bk}]^T$, and $\hat{s}_k=[s_{1k},\ldots,\hat{s}_{Bk}]^T$. Next, with local combining v_{bk} (LMMSE), after deterministic LSFD combining vector a_k, the Use-and-then-Forget (UatF) [10, 11] bounded uplink SINR of IoT-device k for the aforementioned scheme can be represented as a generalized Rayleigh quotient as follows:

$$\mathbf{\Gamma}_{\mathrm{k}}^{\mathrm{UatF}} = \frac{p_k|\mathbf{a}_k^H\mathbf{s}_k|^2}{\mathbf{a}_k^H\big(\sum_{i\neq k}p_i\,\mathbb{E}\{\mathbf{v}_{bi}^H\mathbf{Q}_i\mathbf{Q}_i^H\mathbf{v}_{bi}\}_{b\in|B|} + \sigma^2\mathbf{D}_k\big)\mathbf{a}_k} \tag{9}$$

where, $s_k=E\{v_{bk}^{H}\,Q_k\}_{b\,\in\,|B|}$) is the mean effective channel for IoT-device k, Q_i denotes the effective channel for the interfering IoT-device i (the contribution of IoT-device i interference to IoT-device k), p_i is the uplink transmit power of the IoT-device i, the operator $|\,.\,|$ is the vector norm (Frobenius), v_{bk} is the local combining vector intended for IoT-device k at BS b, and $D_k=diag(E\{|v_{bk}|^2\}_{b\in|B|})$, which for independent BSs, the off-diagonal entries $[D_k]_{j\neq b}$, are zeros. The denominator collects interference and noise covariances at BS outputs.

The vector a_k in (9) denotes the LSFD combining coefficients for IoT-device k, which are deterministic and designed solely based on large-scale channel statistics (e.g., path loss, shadowing, and long-term RIS statistics), and hence remain fixed within each coherence block and independent of the instantaneous small-scale fading realizations. The optimal LSFD weights a_k maximize the instantaneous SINR of each IoT-device in (9), so it can be determined through forcing the derivative w.r.t. a_k* to be zero, $(\partial_{\Gamma k})/(\partial_{ak}{}^*)=0$, $ak^*=arg\ max\text{-}(a_k)\,\{\Gamma_k^{UatF}\}$. For fixed local combiners $\{v_{bk}\}$, powers $\{p_k\}$ and ϕ, the problem of the centralized LSFD vector a_k reduces to maximizing a generalized Rayleigh quotient for each IoT device k. The closed-form solution is obtained by using the generalized eigenvector that corresponds to the biggest eigenvalue. For fixed uplink powers $\{p_k\}$ and RIS phases ϕ, the optimal LSFD vector that maximizes SINR_k is given by the MMSE receiver:

$$\begin{aligned}\mathbf{a}_k^{\star} = \Big(\sum_{\substack{i\in|K|,\\ i\neq k}} \underbrace{p_i\mathbb{E}\{\mathbf{v}_{\mathrm{bk}}^{\mathrm{H}}\,\mathbf{Q}_{\mathrm{k}}\,\mathbf{Q}_{\mathrm{k}}^{\mathrm{H}}\,\mathbf{v}_{bk}\}_{b\in|B|}}_{\substack{\text{inter-IoT-device}\\ \text{covariance matrix}}} \\ +\sigma^2\mathbf{D}_k\Big)^{-1}\sqrt{p_k}\mathbf{s}_k\,,\end{aligned} \tag{10}$$

Where a larger inter-IoT device covariance matrix means more residual interference. For the IoT-device k, the deterministic Large-Scale Fading Decoding vector (LSFD) performs a second-stage linear combining across the locally processed signals of all base stations $a_k\in C^B$. This combining weight is designed solely based only on large-scale statistics (path loss, shadowing, and long-term RIS statistics). It does not depend on instantaneous small-scale fading; hence, it is deterministic and remains fixed within each coherence block. Under the UatF bound, this determinism is essential; it allows separation of mean signal and interference powers. It is worth noting that, reflecting surface dimension N only affects the large-scale statistics entering s_k and inter-IoT-device covariance but not affects the LSFD dimension. Since s_k, D_k, and inter-IoT-device covariance all depend only on large-scale channel statistics, the MMSE-LSFD vector a_k is deterministic and can be computed offline. The statistics in s_k and inter-IoT-device covariance naturally incorporate the long-term RIS response while preserving the deterministic nature of the LSFD weights. Since all expectations are taken with respect to the small-scale fading, the MMSE-LSFD vector depends only on large-scale channel statistics and is therefore deterministic. The closed-form SINR for IoT-device k is then obtained by substituting equation (10) into equation (9):

$$\begin{aligned}\mathbf{\Gamma}_{\mathrm{k}}^{\mathrm{UatF}} = \mathbf{s}_k^H\Big(\sum_{i\in|K|,\,i\neq k} p_i\,\mathbb{E}\{\mathbf{v}_{bk}^H\mathbf{Q}_k\mathbf{Q}_k^H\mathbf{v}_{bk}\}_{b\in|B|} \\ +\sigma^2\mathbf{D}_k\Big)^{-1}\mathbf{s}_k\end{aligned} \tag{11}$$

So, under the UatF bound, the uplink SINR admits the closed-form expression in (11), which is maximized by the MMSE-LSFD vector in (10), with LMMSE local combining affecting only the underlying second-order statistics, i.e., LSFD mainly exploits macro-diversity (channel statistical quantities) to get a smaller inter-IoT-device covariance matrix. The k^{th} IoT-device sum rate (in nats/sec/Hz) is thus represented by the following expression: $R_k=(\tau_u/\tau_c)\,ln(1+\Gamma_k^{UatF})$, where, τ_u is uplink data fraction of the coherence interval length, $\tau_c=\tau_u+\tau_u$.

3.2. PROBLEM FORMULATION

The study aims to enhance the minimum IoT-device achievable rate, or equivalently, the minimum SINR subject to per-device and total transmit power constraints. The essential challenge in cell-free IoT networks with WTIE lies in the complex coupling between three fundamental design aspects: the uplink transmitted power allocation, the distributed large-scale fading decoding (LSFD) combining at the CPU, and the downlink wireless energy harvesting beamforming (EH-BF) at the BSs. These variables are mutually dependent over energy causality constraints and interference-limited performance metrics.

In particular, each IoT device's maximum uplink transmit power budget is determined by the energy captured from downlink beamforming, and the uplink power allocation influences the possible spectral efficiency (SE) through interference management. Simultaneously, the LSFD combining weights must be optimized to suppress both inter-device interference and noise, with their effectiveness depending on the uplink power levels. This creates a circular dependency that prevents straightforward decoupled optimization. In order to overcome these difficulties, the job is rewritten by adding a slack variable (SINR threshold) and using bisection search in conjunction with an alternating optimization framework to solve it. Convex second-order cone programming (SOCP) subproblems with respect to one variable block and fixing the rest comprise each iteration. The main system objective is:

$$\mathcal{P}_0: \max_{\boldsymbol{\phi},\mathbf{V},\mathbf{p},\{\mathbf{a}_k\}} \min_k f_0(\boldsymbol{\phi}, \mathbf{V}, \mathbf{a}_k, p_k) \tag{12}$$

$$\text{subject to: } C1:\ 0 \le p_k \le P_k^{\max}, \quad \forall k$$

$$C2:\ \sum_{k\in|K|} \mathbb{E}\{\| \mathbf{v}_{bk} \|^2\} \le P_b^{\max}, \quad \forall b$$

$$C3:\ \ |\phi_n| = 1, \quad \forall n$$

$$C4:\ \eta_k \left(\sum_{b\in|B|} \|\mathbf{v}_{bk}^H \mathbf{F}_{bk}\|_F^2 + \rho \| \boldsymbol{\phi}\mathbf{H}_{r,k} \|^2 \right) \ge E_k^{\min}, \forall k$$

where, $f0\ (\phi, V, a_k, p_k)=\tau_u\ ln(1+\Gamma_k\ (\phi, V, a_k, p_k)$ [nats/s/Hz], Using hardening bound, η_k is the device energy conversion efficiency, C4 represents energy harvesting constraint with efficiency η_k, and E_k^{req} is the minimum energy required by the IoT sensor for regular performance,

$$E_k^{req} = \tau_p\ p_k^p + \tau_u\ p_k, \text{ and: } E_k^{min} = \tau_u\ p_k + E_k^{circuit} \tag{13}$$

Due to rectifier inefficiencies and diode saturation at high input power, the conversion of RF power to DC energy in practical RF energy harvesting circuits is nonlinear. While a linear model with an efficiency factor η_k captures the low-power regime, for generality, a sigmoidal nonlinear model will be considered, where the harvested energy saturates at a maximum value E_k^{max}. Furthermore, for wireless transfer of information and energy (WTIE), both time-switching (TS) and power-splitting (PS) architectures can be considered, where a fraction of time or received power is allocated to energy harvesting [8]. A common sigmoid or logistic model is: $E_k=(E_k^{max})/(1+e^{ak}\ (P_k^{in}-b_k))$, where, E_k is the harvested DC energy at IoT-device k, E_k^{max} is the maximum harvested or saturation energy, $P_k^{in}=\sum_{b\in|B|} \|v_{bk}^H\ F_{bk}\|_F^2 +\rho\ \|\phi H_{rk}\|^2$, is the total received RF power, a_k is the steepness of the sigmoid, b_k is the midpoint of the logistic curve. The utility function to be maximized in P_0 of eq.(12) is the minimum SE, and this task, in turn, is equivalent to maximizing the minimum SINR, since the function $ln(1+\Gamma_k\ (\phi, V, a_k, p_k))$ is strictly increasing in Γ_k for $\Gamma_k \ge 0$. Therefore, for any fixed feasible power allocation p_k, both terms, $min_k\ ln(1+\Gamma_k\ (\phi, V, a_k, p_k))$, and $ln(1+min_k\ \Gamma_k(\phi, V, a_k, p_k))$ represent complementary formulations of the same underlying SINR balancing and power minimization objectives. Without loss of generality, the max-min SINR in problem $P0$ can be expressed by defining a new slack variable t as the minimum required or target SINR for IoT-device k Γ_k^{min} as follows:

$$\mathcal{P}_1: \quad \max_{\mathbf{a}_k, p_k, \mathbf{v}_{bk}, \boldsymbol{\phi}} t \tag{13}$$

$$\text{subject to: } C1:\ \Gamma_k^{\min} \ge t, \quad \forall k$$

$$C2:\ 0 \le p_k \le P_k^{\max}, \quad \forall k \in /K/$$

$$C3:\ \sum_{k\in/K/} \mathbb{E}\{\| \mathbf{v}_{bk} \|^2\} \le P_b^{\max}, \quad \forall b \in /B/$$

$$C4:\ /\phi_n/ = 1, \quad \boldsymbol{\phi} = \mathrm{diag}\left(e^{j\theta_n}\right), \forall n \in /N/$$

$$C5:\ \eta_k \left(\sum_{b\in/B/} /\!/\mathbf{v}_{bk}^H \mathbf{F}_{bk} /\!/_F^2 + \rho \| \boldsymbol{\phi}\mathbf{H}_{r,k} \|^2 \right) \ge E_k^{\min}, \forall k$$

where, t is the minimum SINR target, $a_k \in C^B$ is the LSFD vector for IoT-device k, p_k is the uplink transmit power of IoT-device k, $v_{bk} \in C^M$ is the wireless EH beamformer from BS b to IoT-device k, η_k is the energy harvesting efficiency of IoT-device k, ρ is the RIS reflection coefficient, τ_u is the uplink transmission time, $E_k^{circuit}$ is the circuit power consumption of IoT-device k. Problem $P1$ is non-convex due to coupling between p_k, v_{bk}, a_k, and ϕ. However, alternating optimization (AO) technique can be employed to optimize one block at a time while keeping others fixed.

3.3. UPLINK POWER CONTROL SUBPROBLEM

The quadratic transform for the SINR inequality in the first constraint $C1$ of P_1 can be obtained through rearranging it to a linear or a convex Second-Order Cone (SOC) form using standard techniques. In other words, to satisfy the max-min SINR target t while respecting per-IoT-device power budgets, the SINR constraints $\Gamma_k^{min} \ge t$ have to be reformulated as a convex SOCP. Using the multidimensional complex quadratic transform, the fractional SINR constraints in problem P_1 with the aid of eq. (11) can be handled as follows:

$$p_k |\mathbf{a}_k^H \mathbf{Q}_k|^2 \ge t \left(\sum_{i\ne k} p_i\ |\mathbf{a}_k^H \mathbf{Q}_i|^2 + \sigma^2\ \|\ \mathbf{a}_k\ \|^2 \right), \tag{14}$$

where, $p_k\ |a_k^H\ Q_k\ |^2$ is the signal power, and $|a_k^H\ Q_i\ |$ is the effective channel gain after LSFD combining for device i as seen by IoT-device k's combiner.

The right-hand side is the total interference-plus-noise power for IoT-device k can be written as (squared Frobenius norm representation):

$$\sum_{i\neq k} p_i \,|\mathbf{a}_k^H \mathbf{Q}_i|^2 + \sigma^2 \parallel \mathbf{a}_k \parallel^2 = \left\| \begin{matrix} \sqrt{p_1}|\mathbf{a}_k^H \mathbf{Q}_1| \\ \sqrt{p_2}|\mathbf{a}_k^H \mathbf{Q}_2| \\ \vdots \\ \sqrt{p_K}|\mathbf{a}_k^H \mathbf{Q}_K| \\ \sigma \parallel \mathbf{a}_k \parallel \end{matrix} \right\|_F^2 = \left\| \begin{matrix} \{(a_k^H \mathbf{Q}_i)\sqrt{p_i}\}_{i\neq k} \\ \sigma \parallel \mathbf{a}_k \parallel_2 \end{matrix} \right\|_F^2 \quad (15)$$

Put (15) back in (14) and rearrange the inequality to yield:

$$\left\| \begin{matrix} \{(a_k^H \mathbf{Q}_i)\sqrt{p_i}\}_{i\neq k} \\ \sigma \parallel \mathbf{a}_k \parallel_2 \end{matrix} \right\|_F \leq \frac{1}{\sqrt{t}} \{a_k^H \mathbf{Q}_k \sqrt{p_k}\},$$

where, $0 \leq p_k \leq P_{max}$). This inequality is a convex SOC constraint in $\{p_k\}$, so it can be solved efficiently using standard solvers. Consequently, the joint optimization problem P_1 can be reformulated as follows:

$$\mathcal{P}_2: \max_{\{p_k\},t} t \quad \text{subject to: } C_1': \sqrt{(p_k)}\, |a_k^H Q_k| \geq \sqrt{t}\| Y_k \|_2,\ C1, C2. \quad (16)$$

where the diagonal interference matrix is, $Y_k = [\{(a_k^H Q_i)\sqrt{(p_i)}\}_{(i\neq k)}, \sigma\|a_k\|_2]$. The max-min SINR optimization is equivalent to a sequence of convex power-minimization SOCPs under fixed SINR targets. Once $\phi^{(n)}$ is fixed, maximizing SINR is equivalent to minimizing total power while satisfying the SINR constraints. This gives:

$$\mathcal{P}_3: \min_{\{p_k\}} \sum_{k\in|K|} p_k \quad \text{subject to: } C1': \sqrt{(p_k)}|a_k^H Q_k| \geq \sqrt{t}\| Y_k \|_2,\ C2,\ C3 \quad (17)$$

3.4. EH DOWNLINK BEAMFORMING SUBPROBLEM

To capture practical RF-DC conversion, a nonlinear logistic energy harvesting model is adopted. Since the harvesting function is monotonic, the EH constraint can be equivalently inverted into a minimum received-power constraint, which admits a standard second-order cone representation for fixed RIS phases. Hence, the resulting EH beamforming subproblem remains convex and can be efficiently solved as an SOCP within the AO framework. The energy harvesting constraint C5 in eq. (14) for the linear EH model can be reformulated as follows:

$$\left(\sum_{b\in|B|} \|\mathbf{v}_{bk}^H \mathbf{F}_{bk}\|_F^2 + \rho \parallel \boldsymbol{\phi}\mathbf{H}_{rk} \parallel^2 \right) \geq \frac{E_k^{\min}}{\eta_k}, \forall k \quad (18)$$

Or in simpler form: $\parallel \boldsymbol{\chi}_k \parallel_F^2 + \rho \parallel \boldsymbol{\phi}\mathbf{H}_{rk} \parallel^2 \geq \frac{E_k^{\min}}{\eta_k}, \forall k,$

where, $\boldsymbol{\chi}_k = \begin{bmatrix} \mathbf{v}_{bk}^H \mathbf{F}_{bk} \\ \mathbf{v}_{bk}^H \mathbf{F}_{bk} \\ \vdots \\ \mathbf{v}_{bk}^H \mathbf{F}_{bk} \end{bmatrix}_F$, and $\sum_{b\in|B|} \|\mathbf{v}_{bk}^H \mathbf{F}_{bk}\|_F^2 = \parallel \boldsymbol{\chi}_k \parallel_F^2$.

which in turns can be rewritten as a convex SOC constraint Frobenius norm representation after taking the square root (both sides are nonnegative):

$$\left\| \{\mathbf{v}_{bk}^H \mathbf{F}_{bk}\}_{b\in|B|} \right\|_F \geq \sqrt{\frac{E_k^{\min}}{\eta_k}}, \forall k \quad (19)$$

This constraint is a standard and convex SOC inequality in $\{p_k\}$, so it can be solved efficiently using standard solvers (CVX-ready). On the other hand, employing eq. (13), the nonlinear EH threshold is:

$$\left\| \{\mathbf{v}_{bk}^H \mathbf{F}_{bk}\}_{b\in|B|} \right\|_F \geq \frac{1}{\sqrt{\rho_k}} \sqrt{\frac{1}{a_k} \ln\left(\frac{E_k^{\max}}{E_k^{\min}} - 1\right) + b_k}, \forall k, \quad (20)$$

where the variable $\rho \in [0,1]$ is the fraction of power for EH in case of employing the power-splitting mode. The downlink EH beamforming subproblem becomes:

$$\mathcal{P}_4: \min_{\{\mathbf{v}_{bk}\}} \sum_{b\in|B|} \sum_{k\in|K|} \parallel \mathbf{v}_{bk} \parallel_F^2 \quad (21)$$

subject to: $C\,5: \|\chi_k\|_F^2 + \rho\|\phi H_{rk}\|^2 \geq E_k^{min}/\eta_k, \forall k \in |K|$

which is also a convex SOCP problem, the objective is a convex quadratic, the constraints are affine in squared norms. This enforces the energy-causality constraints induced by the uplink max-min SE objective, and its feasibility determines whether a candidate SINR target is achievable within the AO-bisection framework. Therefore, the feasibility of the downlink EH problem is monotone in the SINR target justifying and ensuring convergence of the bisection search.

3.5. RIS PHASE SHIFT OPTIMIZATION SUBPROBLEM

The RIS phase optimization is solved via Riemannian gradient ascent on the complex unit-modulus manifold M, guaranteeing feasibility at every iteration. The manifold gradient ascent update produces a non-decreasing surrogate objective and preserves the feasibility of the SINR constraints in the AO-bisection loop. The expected combined channel gain from eq. (3) can be defined as follows:

$$U_{k,i} \triangleq a_k^H E\{Q_i\} = A_{k,i} + B_{k,i}^H \phi, \quad (22)$$

where, $A_{k,i} = a_k^H F_i$, and $B_{k,i} = G_i^H a_k$. Moreover, the covariance matrix of the effective channel component for IoT-device i becomes:

$$a_k^H E\{Q_i Q_i^H\} a_k = \phi^H R_{k,i} \phi + 2Re\{r_{k,i}^H \phi\} + d_{k,i} \quad (23)$$

where the second-order covariance-like matrix of the effective cascaded RIS channel after LSFD weighting, $G_i^H a_k$ is denoted by $R_{k,i} = E\{G_i^H a_k a_k^H G_i\}$ and it is Hermitian positive semidefinite (PSD) matrix $R_{k,i} \succcurlyeq 0$ which captures the power coupling or spatial correlation between RIS elements as seen through the BS combiner. The vector $r_{k,i} \in C^N$, is the cross-correlation vector between the RIS-side cascaded effective channel, and the BS-side direct channel after LSFD combining i.e., $r_{k,i} = E\{G_i^H a_k a_k^H F_i\}$, so it measures coherent coupling between RIS-reflected

path and Direct BS path. If these paths are statistically independent then r_{ki}=0. The total average received power from all IoT-devices (including IoT-device itself) that arrives via the direct IoT-device-to-BS paths, after processing by the LSFD combiner a_k is denoted by the real, non-negative scalar $d_{k,i} \in R_+$, $d_{k,i} = a_k^H E\{F_i F_i^H\} a_k$.

3.6. SINR CONSTRAINT UNDER BISECTION TARGET

For a given target SINR t, the SINR constraint of eq. (14) is equivalent to,

$$p_k \left|U_{k,k}\right|^2 \geq t\left(\sum_{i\neq k} p_i\, a_k^H \mathbb{E}\{Q_i Q_i^H\} a_k + \sigma^2 \parallel a_k \parallel^2\right) \quad (24)$$

The rearranged feasibility SINR constraint after collecting quadratic terms in ϕ can take the form:

$$\phi^H M_k \phi + 2Re\{m_k^H \phi\} \geq t(d_k + \sigma^2 \parallel a_k \parallel^2) - C_k \quad (25)$$

where the matrices M_k and vectors m_k arise from rewriting the UatF SINR constraints as quadratic forms in the RIS phase vector and depend explicitly on the current bisection target t, they collect all RIS-dependent signal and interference terms, these are, respectively:

$$M_k = p_k G_k^H a_k a_k^H G_k - t \sum_{i\in|K|} p_i\, G_i^H a_k a_k^H G_i \quad (26)$$

$$m_k = p_k G_k^H a_k a_k^H F_k - t \sum_{i\in|K|} p_i\, G_i^H a_k a_k^H F_i \quad (27)$$

The constant C_k in (25) is related to the signal power term from the direct path $p_k\, |a_k^H\, E\{F_k\}|^2$ non-RIS i.e., it is the coherent desired-signal power under the UatF bound and therefore appears as a constant offset in the quadratic SINR constraint (separates RIS-dependent vs RIS-independent terms), C_k=0 when the direct link is blocked. The real, non-negative scalar $d_k = \sum_{i\in|K|} p_i\, d_{k,i}$, is the total average received deterministic interference power from all IoT devices (non-coherent terms) scaled by the user transmit powers (including IoT device itself) that arrives via the direct IoT-device-to-BS paths, it is independent of the RIS configuration ϕ i.e., the constant term on the right-hand side of (25) is irrelevant for the gradient computation w.r.t ϕ.

3.7. EUCLIDEAN GRADIENT FOR MANIFOLD OPT.

In the proposed algorithm, a surrogate objective is maximized to find a feasible point that meets the SINR target t. A suitable objective is the sum of the left-hand sides of the per-IoT-device quadratic constraints of inequality (25). From the feasibility test at a fixed target t, define the aggregate function, given a real-valued objective function:

$$f(\phi) = \phi^H M\phi + 2Re\{m^H \phi\}, \quad (28)$$

where the aggregated matrices, $M = \sum_{(k\in|K|)} M_k$ and $m = \sum(k\in|K|) m_k$, address the contributions of the desired signal enhancement (through $|a_k^H\, G_k|^2$ and $|a_k^H\, F_k|^2$) and the interference suppression scaled by the SINR target t (through R_k and r_k). Maximizing $f(\phi)$ promotes the satisfaction of the individual SINR constraints. The Euclidean gradient of $f(\phi)$ in the complex domain is required for the Riemannian gradient computation on the unit-modulus manifold $M = \{\phi \in C^N : |\phi_n| = 1, \forall n\}$. Using Wirtinger calculus, the Euclidean gradient of $f(\phi)$ with respect to the complex conjugate ϕ^* (treating ϕ and ϕ^* as independent) is:

$$\nabla_\phi f = 2M\phi + 2m \quad (29)$$

3.8. COMPUTE GRADIENT ON MANIFOLD

The Riemannian gradient is then obtained by projecting the aggregate Euclidean standard (unconstrained) gradient of the objective function in the embedding space onto the Unit-Modulus Manifold, or the tangent space of the manifold M. This can be applied to the RIS phase shifter optimization update. The complex circle manifold for the RIS phase-shift vector is $M = \{\phi \in C^N : |\phi_n| = 1, \forall n\}$. And this is suitable for the unit-modulus constraints on RIS elements where each element satisfies $\phi_n = e^{j\theta_n}$, $\theta_n \in [0, 2\pi)$. The tangent space for the complex circle manifold at point at ϕ is, $T_\phi M = \{z \in C^N : Re\{z_n\, \phi_n^*\} = 0\}$. Where the product is element-wise multiplication.

Algorithm-I; Proposed Iterative AO approach

Input: Channel statistics $\{b_k, C_k, Q_{r,k}\}$, BS power limits P_b^{BS}, RIS coefficients ρ, EH efficiencies η_k, circuit energies $E_k^{circuit}$, tolerance ε_{AO}, ε_{mf}.

Output: SINR t^*, p_k, LSFD vectors a_k, EH-beamformers v_{bk}, RIS phases Φ.

Initialize parameters:

AO iteration index n=0, RIS phases $\Phi^{(0)}$ randomly on the unit circle, LSFD vectors $a_k^{(0)}$, uplink powers $p_k^{(0)} = P_{min}$, ∀k, SINR bounds: t_{min}=0, $t_{max} = t_{max}^{(0)}$.

1. **Repeat** (AO approach Main loop (n)):
2. Bisection approach (on SINR target t): Set, $t = (t_{min} + t_{max})/2$
3. Update Uplink Power Allocation $p_k^{(n+1)}$ using eq. (17) for fixed $a_k^{(n+1)}$ and $\Phi^{(n)}$.
4. Update LSFD coefficients a_k, using closed-form (10) with fixed $\Phi^{(n)}$, $p_k^{(n+1)}$.
5. Update DL EH-Beamforming, $v_{bk}^{(n+1)}$ employing eq. (22) for fix $\Phi^{(n)}$.
6. Update RIS Phase $\Phi^{(n)}$ (Algorithm II) for fixed $p_k^{(n+1)}$ v_{bk}, and $a_k^{(n+1)}$.
7. Compute Minimum Required Energy: $E_k^{min} = \tau_u\, p_k + E_k^{circuit}$
8. Update Bisection limits:
   If EH-problem is feasible: **Then**: $t_{min}^{(n+1)} = t$
   Else: $t_{max}^{(n+1)} = t$, **End If**
9. Bisection convergence check,
   If $|t_{max} - t_{min}| \leq \varepsilon_{AO}$.
   Then: Accept $t^* = t_{min}$, and,

Break bisection loop
End If

10. **Until** bisection converges otherwise update the iteration index, n=n+1.
11. **Return:** Optimal SINR t*, uplink powers p_k, LSFD vectors a_k, EH-beamformers v_{mk} ,RIS phases Φ.

The gradient on the manifold (the Riemannian gradient) is obtained by the orthogonal projection of the Euclidean gradient onto the tangent space:

$$\nabla_M f=Proj_\phi(\nabla_\phi f)=\nabla_\phi f-Re\{\nabla_\phi f\odot\phi^*\}\odot\phi \quad (30)$$

The third step after the gradient step is the retraction onto the manifold: $\tilde{\phi}=\phi+\alpha\nabla_M f$. Then, the normalized retraction onto the manifold is, $\phi_n=\tilde{\phi}_n/|\tilde{\phi}_n|, \forall n$. Where $\nabla M f$ will be the direction associated with the gradient, and α is the size of the search step. The aggregate Euclidean gradient combines contributions from all constraints and objective in standard complex calculus, while the manifold projection ensures that the movement is in directions that preserve the unit-modulus constraints of RIS elements. The projection step removes the component of the gradient that would change the modulus, keeping only the component that affects the phases. The three steps of the Riemannian manifold optimization are described in detail in the pseudocode provided in Algorithm-II. The complete pseudocode for the suggested AO-algorithm is also presented in Algorithm-I. A non-decreasing SINR feasibility region is produced by each AO step, which optimizes one variable block while holding the others constant.

Algorithm-II; Riemannian Manifold Gradient Descent.

Input: EH-beamformers v_{bk}, ε_{mf}.

Output: Optimal RIS phases Φ*.

Initialize parameters: $\Phi^{(0)}$, m=0

1. **Repeat** Manifold Optimization inner loop (m):
2. Compute Euclidean Gradient w.r.t Φ, $\nabla(\phi^* \Gamma_{min}(\Phi)=\sum_{k\in|K|} 2(M_k \Phi+m_k)$.
3. Update Riemannian gradient: $grad_R \Gamma_{min}(\Phi)$ $=\nabla\Phi \Gamma_{min}$-Rel.{$\nabla_\phi \Gamma_{min}.\Phi^*$}.$\Phi$,
4. Update phase shift: $\Phi^{m+1}=$ $Ret\Phi(\alpha\, grad_R \Gamma_{min}^{(m)})=vect.[(\Phi^{(m)}+\alpha\,\eta^{(m)})$ $/|(\Phi^{(m)}+\alpha\,\eta^{(m)})|]$.
5. Quantize Φ to the nearest points in the φ_{rn} set.
6. Check Manifold convergence: $\varepsilon_{mf} \geq \|\Phi^{(m+1)}-\Phi^{(m)}\|F$
7. m=m+1
8. **Until** Manifold converges
9. **Return**: Optimal RIS phases Φ*= $\Phi^{(m)}$.

- *Riemannian gradient of the SINR on the unit-modulus manifold in step 3 is the projection of* $\nabla_{\phi^*} f(\Phi)$ *onto the tangent space,*
- *phase shift updating in step 4 is performed via descent and retraction of a tangent vector* $\alpha\,\eta^{(m)}$ *at the current point* $\Phi^{(m)}$ *to the unit circle space,* α *is the size of the search step, and* η *is the direction associated with* $grad_R \Gamma_{min}(\Phi)$.

4. COMPUTATIONAL COMPLEXITY

The computational complexity of the proposed methods will depend on the number of alternating optimization (AO) iterations and their level of difficulty (required to solve each subproblem). The BS beamforming subproblem's complexity is polynomial in K in dense cell-free systems with many IoT-devices. However, because the RIS optimization complexity rises linearly with N, the algorithm can effectively handle a large number of RIS elements. For every iteration, the complexity of solving the SOCP for the BS beamforming task is, $O((MBK^2)^2\sqrt{\text{MBK}})=O(K^{4.5}(MB)^{2.5})$. The RIS passive beamforming computation cost is $O(K^2N)$ which is updated via Euclidean gradient. Consequently, the alternating algorithm's total complexity per iteration, $O(NK^2+I_{AO}\, log2\,(1/\varepsilon)((\text{MB})^{2.5}\,K^{4.5}))$ where ε is accuracy of the variable updating and I_{AO} signifies the number of iterations of the AO algorithm to converge.

5. NUMERICAL RESULTS

This section presents simulation results that evaluate the following system configurations for comparative analysis:

- The proposed optimized RIS aided cell-free MIMO IoT scheme, namely, AO-IVT, where the scheme variables are optimized utilizing Algorithm I, while the RIS phase shifts are refined through Algorithm II.
- AO-IVT (no power control) where in this benchmark, IoT devices were assigned equal power, with the other variables designed using Algorithm-II.
- Random ϕ and Equal p, in which the reflecting surface phase shift angles are selected arbitrarily in the range $\phi\in(0,2\pi]$.
- The traditional CF-MIMO IoT system without employing the reflecting surface assistant.
- The SDR-WMMSE scheme, which merges the robust Weighted Minimum Mean Square Error technique with Semidefinite Relaxation to tolerate the non-convex, NP-hard constraints for the power control in CF-MIMO systems.

Without loss of generality, the structure is assumed to include BSs and RISs that are uniformly spread in circles (within a radius of 400 m) about the IoT-devices. The various single-antenna IoT-devices are positioned with uniform distribution in a circle of radius 20m. For the model of the propagations, a distance-dependent channel path loss is assumed, and for the small-scale fading model, a Rician fading channel of factor 4 is adopted, with the simulation settings based on prior research. For the energy-consuming model, the static or fixed energy

costs of the hardware circuit per BS and IoT device are, respectively, (P_b^{BS}, P_k^{UE}) {10 dB and 10 dBm}. The hardware energy costs per reflecting element for {1, 3, 4, and infinite} phase shift resolution bits are, respectively, {10, 15, 20, and 25} dBm. The numerical results for channel realizations and network architecture both are averaged over 4×10^2 trials with a convergence tolerance of $\epsilon=10^{-4}$ and a minimum SINR {t} of 0 dB, noise variance is -96 dBm. Each coherence interval consists of τ_c=200 symbols (pilot-training length τ_p=10 symbols, uplink data transmission length τ_u=190 symbols), the path loss exponent is set to {2.3, 2.5, and 3.5} for the BS-IRS channel, device-IRS channel, and the direct channel, respectively. The values of additional parameters, BS antennas M, number of IoT devices K, and number of RIS elements N) will all be specified within each simulation figure.

5.1. RATE-OUTAGE PROBABILITY ANALYSIS

The cumulative distribution function (CDF) provides crucial insights into the distribution of performance metrics, reflecting the probability that all IoT devices simultaneously satisfy a QoS requirement and characterizing IoT device fairness and reliability beyond average metrics. Therefore, the simulation will evaluate the CDF of the minimum achievable rate (or equivalently, SINR). Specifically, the rate outage probability is defined as $P_{outage}(R_0) = Pr\{min(k\in K)\ R_k \le R_0\}$, where $R_k = log_2\ (1+\Gamma_k)$ denotes the attainable uplink rate of IoT device k, and R_0 is a target rate threshold. All simulations have been carried out with $BS = 2$, $K = 5$, $M = 4$, $N = 64$. First, Fig. 2 shows the outage probability (CDF) of the IoT-device uplink rate for the proposed RIS-aided cell-free MIMO scheme and the benchmark schemes; AO-IVT (no power control); Equal p, the traditional cell-free MIMO structure without IRS; and the SDR-WMMSE scheme. The CDF plots for RIS-aided schemes are plotted using 4-bit RIS phase shifting. For the indicated 5% likely rate-outage, the proposed scheme under optimized variables exposes a noteworthy minimum target rate enhancement of almost 83% (minimum rate rises from 0.24 to 1.5 nat/s/Hz) in comparison to a traditional case (equal power and random phase shift), while the20th percentile increases from 0.82 to 2.51 nat/s/Hz.

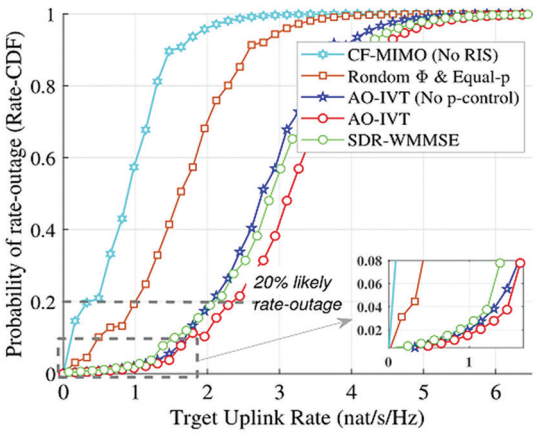


Fig. 2. CDF of the target uplink rate against different schemes

Next, Fig. 3 shows the outage probability results of the scheme simulation across two values of the quantization bits for the discrete phase shift levels. As shown by CDF curves of this figure, e.g., for the 90th percentile, increasing quantization by 2 bits results in almost a 0.5 nat/s/Hz boost in the minimum target rate. Switching from 2-bit to 4-bit IRS phase shifters results in significant performance benefits, which can be attributed to precise phase shift selection. As a result, to build RIS systems and achieve considerable gains over typical cell-free MIMO schemes, there is no necessity for employing expensive high-resolution phase-shift circuits. Fig. 4 (a) shows that the outage probability gap between the proposed scheme (marked as LSFD) and the conventional system (with fixed LSFD coefficients) is approximately 1.2 for a 5% likely rate-outage. In the former approach, the receiver power assignments and the CPU filtering coefficient vectors are made optimal via Algorithm-I, while in the latter approach, they are not optimized.

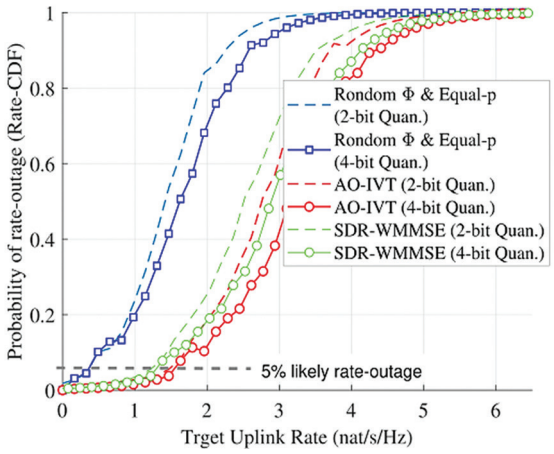
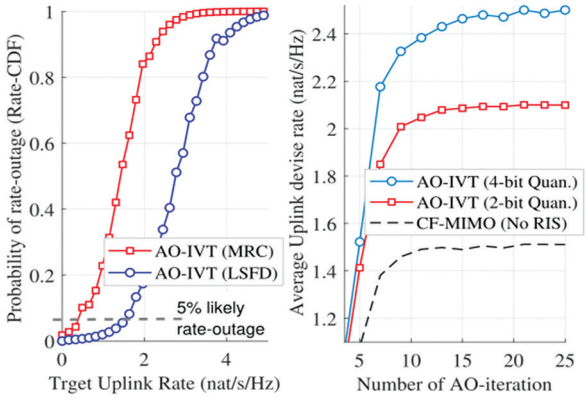


Fig. 3. The target uplink data rate's CDF against the quantization bits for the discrete phase shift levels



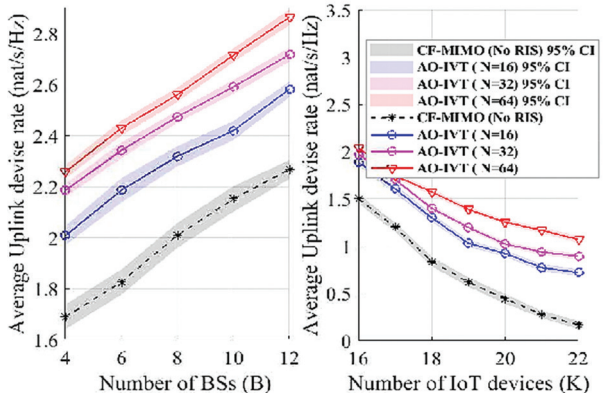
(a) (b)

Fig. 4. (**a**) The target uplink data rate's CDF against different receiving combining approaches. (**b**) Proposed algorithm Convergence performance

The rate convergence behavior of the proposed system is shown in Fig. 4(b). As shown in this figure, about six iterations are sufficient to achieve about 80% of the average rate.

5.2. AVERAGE UPLINK DATA RATE ANALYSIS

The scaling performance of the algorithm with the network size is depicted in Fig. 5. Here, the simulation outcomes are acquired through independent Monte Carlo analyses (N_{MC}=1000 independent realizations of the channel) to confirm statistical resilience. The 95% confidence interval (CI) is determined as follows, CI=1.96·(STD/$\sqrt{N_{sim}}$) where, 1.96 is the Gaussian factor for 95% CI, STD is the standard deviation from simulations, and N_{MC} is the number of Monte Carlo runs. This certifies that the achieved performance improvements are statistically considerable with 95% confidence. First, for a number of $RISs = BSs$, $M = 4$ antennas, Fig. 5(a) depicts that the average uplink data rate increases with the growth in the number of BSs because more BSs can achieve more diversity and antenna gain. In addition, increasing the number of RIS's elements from 16 to 64 elements can carry a notable scheme performance gain (about 13% for B=10 BSs). Next, Figure 5(b) shows the impact of increasing the number of IoT devices on the uplink average rate for B=2 BSs, R=2 $RISs$, M= 4 antennas, N=16, 32, 64 elements, and τ_p=10symbols. As the density of the devices increases in the network, the per-device average data rate decreases since a limited length of the pilot sequence results in an increase in the interference due to pilot contamination. It is worth noting that increasing the number of RIS elements can alleviate the performance decrease caused by the increased number of IoT devices. In actuality, RIS passive-beamforming can improve interference control. This highlights how crucial it is to implement RIS in densified networks.



(a) (b)

Fig. 5. Proposed algorithm performance scalability w.r.t: (**a**) number of Base Stations, (**b**) number of served IoT devices

6. CONCLUSION

This study developed a low-complexity framework for max-min rate optimization in RIS-assisted IoT cell-free MIMO systems. By exploiting the monotonic equivalence between max-min SINR and max-min data-rate, the originally nonconvex problem was reformulated into a sequence of convex SOCP subproblems solvable via an alternating optimization scheme with the intermediate value theorem. The proposed algorithm provides definite convergence to a stationary solution with polynomial per-iteration complexity, making it scalable to large numbers of IoT devices and RIS elements. According to simulation results, the proposed approach outperforms the conventional ones in terms of rate-outage probability. For example, the proposed scheme under optimized variables exposes a noteworthy minimum target rate enhancement of almost 83% (minimum rate rises from 0.24 to 1.5 nat/s/Hz) in comparison to a traditional case (equal power and random phase shift), while the 20th percentile increases from 0.82 to 2.51 nat/s/Hz. The theoretical study and numerical results yield key conclusions that can be applied to address the aforementioned challenges in the design of RIS-assisted IoT cell-free systems.

CONFLICTS OF INTEREST

The authors declare that they have no known competing financial interests or personal relationships that could have appeared to influence the work reported in this paper.

DECLARATION OF THE USE OF AI TOOLS

"No artificial intelligence tools were used in the preparation of this manuscript".

REFERENCES:

[1] X. Li, M. Zhang, H. Chen, C. Han, L. Li, D. T. Do, A. Nallanathan, "UAV-enabled multi-pair massive MIMO-NOMA relay systems with low-resolution ADCs/DACs", IEEE Transactions on Vehicular Technology, Vol. 73, No. 2, 2023, pp. 2171-2186. doi: 10.1109/tvt.2023.3315556

[2] Q. Xue, X. Fang, M. Xiao, S. Mumtaz, J. Rodriguez, "Beam management for millimeter-wave beamspace MU-MIMO systems", IEEE Transactions on Communications, Vol. 67, No. 1, 2018, pp. 205-217. doi: 10.1109/TCOMM.2018.2865749.

[3] H. Mohammed, "Internet of Vehicles Security Improvement Based Controller Area Network and Artificial Intelligence", Komunikácie-vedecké listy Žilinskej univerzity v Žiline, Vol. 27, No. 2, 2025, pp. 14-23. doi: 10.26552/com.c.2025.017.

[4] I. Hburi, H. F. Khazaal, "An efficient two-stage user association scheme for green C-RAN systems", Indonesian Journal of Electrical Engineering and Computer Science, Vol. 16, No. 2, 2019, pp. 794-802. doi: 10.11591/ijeecs. v16.i2. pp794-802.

[5] H. A. Ajeel, R. Q. Muhammed, I. S. Baqer, "Enhancing the open-RANs performance with meta-surface technique", Proceedings of the AIP Conference, Vol. 3264, No. 1, 2025, p. 020011. doi: 10.1063/5.0260395.

[6] M. Hassan, K. Hamid, R. A. Saeed, H. Alhumyani, A. Alenizi, "Reconfigurable intelligent surfaces in 6G mMIMO NOMA networks: A comprehensive analysis", International Journal of Electrical and Computer Engineering Systems, Vol. 16, No. 2, 2025, pp. 87-97. doi: 10.32985/ijeces.16.2.8

[7] S. Han, G. Luo, F. Qu, M. Lestas, F. Y. Wang, "Empowering vehicle connectivity-the SOTA and future prospects of reconfigurable intelligent surfaces in mobile communications: A review", IEEE Sensors Journal, Vol. 25, No. 12, 2025, pp. 20789-20806. doi: 10.1109/jsen.2025.3586678.

[8] X. Peng, Q. Tao, X. Gan, C. Zhong, "Intelligent-reflecting-surface-enhanced cell-free symbiotic radio sysems", IEEE Internet of Things Journal, Vol. 10, No. 22, 2023, pp. 19545-19557. doi: 10.1109/jiot.2023.3267658.

[9] S. Zeping, H. Ngo, T. Van Chien, "RIS-assisted cell-free massive MIMO relying on reflection pattern modulation", IEEE Transactions on Communications, Vol. 73, No. 2, 2025, pp. 968-982. doi: 10.1109/tcomm.2024.3446589.

[10] N. Ain, L. Miretti, S. Stańczak, "On the Optimal Performance of Distributed Cell-Free Massive MIMO with LoS Propagation", Proceedings of the IEEE Wireless Communications and Networking Conference, Milan, Italy, 24-27 March 2025, pp. 1-7. doi: 10.1109/wcnc61545.2025.10978201.

[11] A. Khalil, M. Y. Selim, M. A. Rahman, "CURE: Enabling RF Energy Harvesting Using Cell-Free Massive MIMO UAVs Assisted by RIS", Proceedings of the IEEE 46th Conference on Local Computer Networks, Edmonton, AB, Canada, 4-7 October 2021, pp. 533-540. doi: 10.1109/LCN52139.2021.9524984.

[12] S. Mohammed, D. A. Khader, I. Hburi, H. F. Kazal, B. K. Al-Shammari, "A Riemannian Geometry-based Hybrid Beamforming for mmWave Systems", Proceedings of the International Conference on Computer Science and Software Engineering, Duhok, Iraq, 2025, pp. 239-245. doi: 10.1109/csase63707.2025.11054020.